First-principles study of boron oxygen hole centers in crystals: Electronic structures and nuclear hyperfine and quadrupole parameters

Zucheng Li(李祖成)* and Yuanming Pan†

Department of Geological Sciences, University of Saskatchewan, Saskatoon, Saskatchewan S7N 5E2, Canada

(Received 2 May 2011; revised manuscript received 6 July 2011; published 14 September 2011)

The electronic structures, nuclear hyperfine coupling constants, and nuclear quadrupole parameters of fundamental boron oxygen hole centers (BOHCs) in zircon ($ZrSiO_4$, $I4_1/amd$) and calcite ($CaCO_3$, $R\bar{3}c$) have been investigated using *ab initio* Hartree–Fock (HF) and various density functional theory (DFT) methods based on the supercell models with all-electron localized basis sets. Both exact HF exchange and appropriate correlation functionals are important in describing the BOHCs, and the parameter-free hybrid method based on Perdew, Burke, and Ernzerhof density functionals (PBE0) turns out to be the best DFT method in reproducing the electron paramagnetic resonance (EPR) data. Our results reveal three distinct types of simple-spin ($S = 1/2$) $[BO_3]^{2-}$ centers in calcite: (i) the classic $[BO_3]^{2-}$ radical with the D_{3h} symmetry and the unpaired spin equally distributed on the three oxygen atoms (i.e. the O_3^{5-} type); (ii) the previously reported $[BO_2]^0$ center with the unpaired spin equally distributed on two of the three oxygen atoms (O_2^{3-}); and (iii) a new variety with ~90% of its unpaired spin localized on one (O^-) of the three oxygen atoms with a long B-O bond (1.44 Å). Calculations confirm the unusual $[BO_4]^0$ center in zircon and show it to arise from a highly distorted configuration with 90% of the unpaired spin on one oxygen atom that has a considerably longer B-O bond (1.68 Å) than its three counterparts (1.45 Å). The calculated magnitudes and directions of ^{11}B and ^{17}O hyperfine coupling constants and nuclear quadrupole constants for the $[BO_4]^0$ center in zircon are in excellent agreement with the 15 K EPR experimental data. These BOHCs are all characterized by a small negative spin density on the central B atom arising from spin polarization. Our calculations also demonstrate that the spin densities on BOHCs are affected substantially by crystalline environments, and so periodic boundary treatment, such as the supercell scheme, is a must in accounting for the electronic and spin structures of BOHCs in crystals. These atomistic and electronic models of BOHCs in the crystalline matrices provide new insights into their precursors and counterparts in glasses and other amorphous materials.

DOI: 10.1103/PhysRevB.84.115112 PACS number(s): 71.15.Mb, 61.72.Bb, 61.80.Az, 31.15.ej

I. INTRODUCTION

Boron-centered oxyradicals, including both boron oxygen hole centers (BOHCs) and boron electron centers (BECs), are fundamental radiation-induced defects in borate, borosilicate, and borophosphate glasses and are known to profoundly influence the applications of these important materials from fiber optics to long-term disposal of high-level nuclear wastes.[1–17] Electron paramagnetic resonance (EPR) spectroscopic studies of BOHCs and BECs in borate and borosilicate glasses date back to 1950s[1–3,18] and have been continued by using related but more sophisticated techniques, such as pulse electron nuclear double resonance (ENDOR), electron spin echo modulation (ESEEM), and hyperfine sublevel correlation (HYSCORE) spectroscopy.[6,7,11,13–15] These experimental studies along with theoretical investigations[4,11,13,14,19] have established BOHCs, such as $[BO_3]^{2-}$ and $[BO_4]^0$, as the most prevalent defects in borate, borosilicate, and borophosphate glasses. However, questions remain about the atomistic and electronic structures of these BOHCs in glasses.[6,15,20,21]

In this regard, boron-centered oxyradicals in crystalline matrices, which are amenable to investigations by single-crystal EPR and related techniques,[7,21–25] have been important in providing models for analogous defects in glasses. In particular, single-crystal EPR spectra can provide detailed information about the orientation of the paramagnetic species in the host lattice, hence making unambiguous identification and, under favorable conditions, elucidation of the atomistic and electronic structure possible. For example, the classic $[BO_3]^{2-}$ radical established in gamma-ray-irradiated calcite[26] has long been cited as a model for this type of BOHC in glasses and other amorphous materials.[18] Similarly, BOHCs in danburite $CaB_2Si_2O_8$ also provide structural models for similar defects in alkali borosilicate glasses.[7]

However, there remain questions about the atomistic and electronic structures of boron-centered oxyradicals in crystalline matrices as well.[21,25] For example, Li *et al.*[21] noted that the three most common types of BOHC, namely $[BO_4]^0$, $[BO_3]^{2-}$, and $[BO_2]^0$, in crystalline matrices share similar principal g-factor values and A(^{11}B) hyperfine coupling constants (*hfcc*), making their experimental identification difficult. Here, $[BO_4]^0$ and $[BO_3]^{2-}$ are equivalent to $[BO_4]^{4-}$ and $[BO_3]^0$, respectively, owing to different notations used in the EPR literature.[27] We emphasize that neither notation is completely satisfactory because they do not specify the location of the unpaired spin. In this study, we retain the symbols $[BO_4]^0$ and $[BO_3]^{2-}$ for all simple-spin ($S = 1/2$) BOHCs with the central B atom coordinated to four and three oxygen atoms, respectively. Walsby *et al.*[25] noted that their proposed $[BO_4]^0$ center in zircon, which has substantially smaller A(^{11}B) *hfcc* than other $[BO_4]^0$ radicals,[21] is not directly comparable with the well-established center $[AlO_4]^0$. Similarly, the proposed $[BO_2]^0$ centers in calcite[28] and anhydrite[29] have principal A(^{11}B) values similar to those of the $[BO_3]^{2-}$ center and appear to be problematic as well.

We attempt to answer these questions by using supercell first-principles calculations[30] of BOHCs in $ZrSiO_4$ (zircon, $I4_1/amd$) and $CaCO_3$ (calcite, $R\bar{3}c$). The main advantage of the supercell approach over previous theoretical treatments based on free-radical models,[4,26] semi-empirical methods,[7]

or cluster calculations[19] is that we are able to evaluate the effects of crystalline environments on these defects on a rigorous quantum-mechanical basis of crystalline systems.[21] The two hosts are chosen for the fact that high-quality EPR experimental results are available for the three major BOHCs.[25–29] In particular, the $[BO_4]^0$ center in $ZrSiO_4$[25] represents not only an unusual case for this type of defects and is compared with results from the more common $[BO_4]^0$ center in datolite,[21] but also a BOHC with both accurate EPR hyperfine and nuclear quadrupole tensors at low temperature. In addition, BOHCs in the two hosts are well defined in the sense that they are separate from neighboring anions, CO_3^{2-} and SiO_4^{4-}, and so the crystalline effects can be well examined.

In addition, previous studies on the BOHCs in doped silica and the $[AlO4]^0$ center in α quartz showed that the exact Hartree–Fock exchange is important in the localization of the unpaired spin.[19,31,32] However, no reports reproduced both EPR hyperfine and quadrupole tensors, including the magnitudes and directions of the principal axis systems. Therefore, we also intend to evaluate the *ab initio* Hartree–Fock (HF) and available DFT methods to determine the best theoretical method that is able to reproduce the EPR experimental data and thus provide the best theoretical atomistic models for BOHCs.

II. CALCULATION METHODS

A. Crystalline DFT calculation details

All periodical calculations have been performed using the supercell approach[30,33,34] and various DFT methods, including Becke's three-parameter (B3) hybrid density functional methods B3LYP/PW91[35] as implemented in the package CRYSTAL06[36] and the nonempirical parameter free-hybrid method PBE0.[37] Here, PW denotes Perdew and Wang's generalized gradient approximation (GGA) correlation functional,[38] and PBE stands for the Perdew–Burke–Ernzerhof GGA exchange and correlation functionals that contain no empirical parameters.[39] The unrestricted open-shell scheme in self-consistent field (SCF) calculations for the open shell BOHC systems was used because one unpaired electron or spin is involved. The method using B3PW91 is hereafter referred to as P-B3PW for periodic B3PW. Dovesi and Orlando[33] showed that supercells containing 50 to 100 atoms are sufficiently large for adequate description of neutral defects, such as the BOHCs investigated in this study.[27] Our previous calculations also showed that supercells of comparable sizes are capable of describing similar defects satisfactorily.[21,40]

In this paper, we have evaluated three supercells from single $1 \times 1 \times 1$, quadruple $2 \times 2 \times 1$ to octuple $2 \times 2 \times 2$ primitive cells for both hosts. Because the best results are from the largest $2 \times 2 \times 2$ supercell, only these data are discussed below. The single $1 \times 1 \times 1$ cells for calcite and zircon contain only 10 and 12 atoms, respectively, whereas the $2 \times 2 \times 2$ supercells consist of 80 and 96 atoms, respectively.

The basis sets in this paper have been tested in previous solid state calculations. They are basically double-zeta valence plus polarization (DZVP) quality for atoms Ca, Zr, Si, O, and C, but the basis set for boron is of better double-zeta-plus polarization quality (DZP). The Ca basis set is the contracted Gaussian type orbitals (GTOs) [1*s*4s*p*2*d*] from primitive or uncontracted GTOs (21*s*13*p*3*d*)[41] and that for Zr is Dovesi's [1*s*4s*p*3*d*] contracted from (26*s*17*p*9*d*).[42] The Si basis set is Pisani's[43] 8-41G** [1*s*3*sp*2*d*] from (20*s*13*p*2*d*). Basis sets for O and C are 6-31G* with standard contraction of [3*s*2*p*1*d*],[44] while that for B is the def2-TZVP,[45] except that the diffuse functions with exponents less than 0.1 and the outmost *d* and *f* polarization functions are discarded to avoid linear correlation and integration problems in the calculations, and so the actual basis set is [4*s*2*p*1*d*] from (10*s*5*p*1*d*).

The tolerances for Coulomb and exchange sums were initially set to 10^{-7} and 10^{-14} Hartree, respectively, along with a tight SCF tolerance of 10^{-7} for perfect crystals and preliminary defect structure calculations.[21] To examine the performance of various DFT methods on the defect centers, even tighter tolerances of 10^{-8} and 10^{-18} Hartree for the sums and 10^{-8} for SCF have been used. Accordingly, the DFT integration grid was set to the default one (55,434) with 55 radial points and the maximum of 434 angular points at first; then the extra-large grid (XLGRID) that employs the pruned (75,974) grid for each atom was used. All of these parameters are much more accurate in description of the optimized charge and spin densities as well as the defect structures in the crystals and thus better reproduce the EPR experiments than the default ones. The Pack–Monkhorst shrink factor[36] for the single-cell geometry optimization was set to 8, giving different total *k* points for the two crystals in the irreducible Brillouin zone (IBZ). Due to symmetry reduction after the introduction of the defects in the supercells, the shrink factors were reduced to 6 and 4 for supercells $2 \times 2 \times 1$ and $2 \times 2 \times 2$, respectively, which are the largest values allowed by CRYSTAL06 for such crystals. In the single-cell calculations for calcite, shrink factor of 8 turned out to be 105 *k* points in its IBZ, while our largest calculation including 96 atoms for zircon, the shrink factor of 4 for Pack–Monkhorst net resulted in 36 *k* points in IBZ. The Fermi surface of the defect system was described by the Gilat net[36] characterized by another shrink factor, whose value was always taken as the double of the Pack–Monkhorst shrink factor.

Calculations started with the construction and optimization of the unit cells and various supercells for the perfect structures. Subsequently, defects were introduced to the optimized supercells by replacing one C atom in calcite and one Si atom in zircon with a boron atom, and the whole structures were then allowed to relax and were fully optimized. The convergence of defect-related properties (i.e. spin density, defect geometry, and *hfcc*) was evaluated with respect to the supercell sizes and DFT and HF methods.

B. Nuclear hyperfine and quadrupole coupling parameters

After the defect supercells have been optimized, the *hfcc*'s and *nqc*'s for the three magnetic nuclei (^{10}B, ^{11}B, and ^{17}O) were calculated using the hyperfine coupling spin-Hamiltonian,

$$\widehat{\boldsymbol{H}}_{hfc} = \mathbf{S} \cdot \mathbf{A} \cdot \mathbf{I} + \mathbf{I} \cdot \mathbf{P} \cdot \mathbf{I}. \quad (1)$$

Here, **S** and **I** are the electron spin and nuclear spin operators, respectively, and **A** and **P** (3×3 matrices) are the nuclear hyperfine coupling and nuclear quadrupole parameters, respectively. Matrix **A** can be diagonalized in a principal

axis system and expressed in two parts: the isotropic *hfcc* ($a_{\rm iso}$), representing the Fermi contact interaction between the electron spin (**S**) and the nuclear spin (**I**), and the anisotropic *hfcc*'s (T_i) as follows.

$$\boldsymbol{A} = \begin{bmatrix} A_1 & 0 & 0 \\ 0 & A_2 & 0 \\ 0 & 0 & A_3 \end{bmatrix} = a_{\rm iso}\boldsymbol{U} + \begin{bmatrix} T_1 & 0 & 0 \\ 0 & T_2 & 0 \\ 0 & 0 & T_3 \end{bmatrix}. \quad (2)$$

Here, **U** is the 3×3 unit matrix. **T** is traceless and is expressed in three components T_i ($i = xx$, yy, and zz, or simply 1, 2, and 3). T_{zz} (T_3) is usually given the largest absolute T_i value. Diagonalized hyperfine components A_i are derived in EPR and related experiments, as are the $a_{\rm iso}$ and T_i values. The *hfcc* results relate to the spin density by the following formulae,[36]

$$a_{\rm iso} = \frac{(A_1 + A_2 + A_3)}{3} = \frac{2}{3}\mu_0 g_N \beta_N g_e \beta_e \langle \rho^{\rm spin}(\boldsymbol{r}_A)\rangle, \quad (3a)$$

$$T_i = A_i - a_{\rm iso} = \frac{1}{4}\mu_0 g_N \beta_N g_e \beta_e T^A_{ij}\,|_{i=j}\ , \quad (3b)$$

$$T^A_{ij} = \sum_{\mu\nu}\sum_{w} P^{\rm spin}_{\mu\nu w} \int \varphi_\mu(\mathbf{r}) \left(\frac{r_A^2\delta_{ij} - 3r_{Ai}r_{Aj}}{r_A^5}\right)\varphi^w_\nu(\boldsymbol{r})d\boldsymbol{r}, \quad (3c)$$

where μ_0 is the permeability of vacuum, g_N is the nuclear g factor and g_e is the electronic g factor, β_N and β_e are the nuclear and Bohr magnetons, respectively, $\langle\rho^{\rm spin}(\mathbf{r}_{\rm A})\rangle$ is the spin density on the nucleus A at point $\mathbf{r}_{\rm A}$, $r_{\rm A} = |\mathbf{r} - \mathbf{r}_{\rm A}|$, $r_{{\rm A}i} = (\mathbf{r} - \mathbf{r}_{\rm A})_i$, the ith component of vector $\mathbf{r}_{\rm A}$, δ_{ij} is Kronecker delta, and $P^{\rm spin}_{\mu\nu w}$ is the spin density matrix element between basis functions $\varphi_\mu(\mathbf{r})$ of the reference cell and $\varphi^w_\nu(\boldsymbol{r})$ of the wth cell.

The three magnetic nuclei ^{10}B, ^{11}B, and ^{17}O involved in BOHCs have nuclear spins of 3, 3/2, and 5/2, respectively, and so they can interact with the magnetic field for detection by EPR. However, most studies of BOHCs usually do not report the ^{10}B hyperfine coupling constants or nuclear quadrupole, which are difficult to detect owing to ^{10}B's natural isotope abundance of 19.9% and are assumed to be proportional to the ^{11}B counterparts.[25] Similarly, experimental ^{17}O hyperfine coupling constants and nuclear quadrupole parameters are generally not available owing to the exceedingly low abundance of this isotope (i.e. 0.038%). Therefore, our discussions below focus mostly on the ^{11}B hyperfine coupling constants and nuclear quadrupole coupling constants or tensors (*nqc* or **P**).

However, CRYSTAL06 does not calculate **P** directly; it gives the nuclear electric field gradient (EFG) tensor **V**, which can be diagonalized in its principal axis system as a traceless 3×3 matrix. From the diagonal elements, V_{xx}, V_{yy}, and V_{zz}, we can derive the nuclear quadrupole tensor **P** and its related *nqc*'s. The diagonal elements are usually ordered according to their magnitude as $|V_{zz}| \geqslant |V_{yy}| \geqslant |V_{xx}|$; another convention is the one that exchanges the order of V_{xx} and V_{yy}. We use the following equations to obtain the two *nqc*'s,

$$C_Q \equiv \frac{e^2 q Q}{h} = V_{zz}Q, \quad (4)$$

$$\eta_Q = \frac{(V_{xx} - V_{yy})}{V_{zz}}, \quad (5)$$

where C_Q denotes the nuclear quadrupole coupling constant, and *eq* denotes the largest EFG component V_{zz}, and eQ, sometimes written as Q, represents the electric nuclear quadrupole moment.[46] Here, h is Planck constant. The conversion factor of 234.9647 must be multiplied to the product $V_{zz}Q$ if V_{zz} is given in atomic units as CRYSTAL06 does and Q in *barn* in Eq. (4). The quantity η_Q is the asymmetric parameter, which takes values between 0 and 1. Here, η_Q describes the asymmetry of the electron charge density distribution around the nucleus away from the axial symmetry. C_Q and η_Q are usually obtained from the nuclear magnetic resonance (NMR) experiment, but they are also given in many EPR experiments.

In EPR experiments, the nuclear quadrupole coupling interaction with a nuclear spin I greater than 1/2 is expressed in tensor **P**. The three diagonal elements are commonly denoted as P_1, P_2, and P_3, where the subscripts stand for the principal axes 1, 2, and 3, respectively. The magnitude of P_i's commonly follows the above EFG tensor **V** convention: P_3 is given the largest absolute value. The three components for a nucleus with the nuclear spin quantum number I are calculated as follows,[47]

$$P_3 = \frac{C_Q}{[2I(I-1)]}, \quad (6a)$$

$$P_1 = -\frac{(1-\eta_Q)}{2}P_3, \quad (6b)$$

$$P_2 = -\frac{(1+\eta_Q)}{2}P_3. \quad (6c)$$

C. Directions of hyperfine and nuclear quadrupole coupling tensors

For both anisotropic *hfcc* and *nqc* components, CRYSTAL06 can give the direction cosines of each of their own principal axes in the standard Cartesian coordinate system used in the wave-function calculation of the program. We thus use the direction cosines, e.g. $\cos(\alpha_\lambda)$, $\cos(\beta_\lambda)$, $\cos(\gamma_\lambda)$ of axis λ in the principal axes system of **T**, **A**, or **P** to derive the corresponding polar and azimuthal angles θ_λ and ϕ_λ that are commonly reported in EPR experiments. Since these direction cosines have already defined the axis λ in the principal axes system, that is, in this system, the tensor is diagonalized, so we only need to transform the axis λ from the three direction angles into the spherical polar and azimuthal angles. To do this, we just have to establish the relationship between the direction cosines with three coordinates of a unit vector $\mathbf{U}_\lambda$ that stands for the principal axis λ in the standard Cartesian coordinate system. Suppose the three Cartesian coordinates of the unit vector $\mathbf{U}_\lambda$ of principal axis λ are x_λ, y_λ, and z_λ, then we have the following relations,

$$x_\lambda = \cos(\alpha_\lambda); \quad y_\lambda = \cos(\beta_\lambda); \quad z_\lambda = \cos(\gamma_\lambda). \quad (7)$$

With this connection, we can derive the polar and azimuthal angles θs_λ and ϕ_λ of principal axis λ using the conventional transformation of the coordinates from the standard Cartesian coordinate system to the spherical polar system,

$$\theta_\lambda = \arccos(z_\lambda) = \gamma_\lambda; \quad \phi_\lambda = \mathrm{atan2}(y_\lambda, x_\lambda). \quad (8)$$

TABLE I. Bond length (Å), spin (e), ^{11}B hyperfine (mT) and quadrupole (C_Q in MHz) parameters and formation energies (eV) of $[BO_3]^{2-}$(**I**) in calcite.

	$2\times2\times1$[a]	$2\times2\times2$[a]	$2\times2\times2$[b]	Mol.[b]	EPR[c]	EPR[d]
r(B-O_1)	1.348	1.353	1.355	1.375		
r(B-O_2)	1.356	1.353	1.355	1.375		
r(B-O_3)	1.360	1.357	1.355	1.375		
Spin B	−0.095	−0.095	−0.095	−0.160	−0.085	
Spin O_1	0.304	0.354	0.363	0.387	0.362	
Spin O_2	0.373	0.354	0.363	0.387	0.362	
Spin O_3	0.414	0.382	0.363	0.387	0.362	
$A_{zz}/g_e\beta_e$	−1.211	−1.207	−1.207	−1.217	−1.26	(−)1.28
$A_{xx}/g_e\beta_e$	−0.788	−0.770	−0.776	−0.760	−0.83	(−)0.80
$A_{yy}/g_e\beta_e$	−0.756	−0.759	−0.776	−0.760	−0.83	(−)0.80
$a_{iso}/g_e\beta_e$	−0.915	−0.912	−0.913	−0.919	−0.98	(−)0.96
C_Q/h	2.6848	2.6884	2.6758	2.6985	2.6[e]	
η_Q	0.0863	0.0284	0.0000	0.0000	0.0[e]	
E_{form}[f]		0.9614	0.9749			

[a]Supercell asymmetric P-B3PW results of this work.
[b]P-B3PW D_{3h} results of this work; Mol. for free radical $[BO_3]^{2-}$ B3PW/6-311G** results.
[c]77 K EPR data from Ref. 26.
[d]298 K EPR data from Ref. 53; we add the signs in parentheses.
[e]NMR results for the BO_3 group in calcite from Ref. 54.
[f]E_{form} was defined in Eq. (9), and XLGRID and tight convergences were used.

Here, atan2 is a variation of trigonometric arctangent function, and it gives the azimuthal angle in radians for real Cartesian coordinates. Of course, EPR experiments do not give absolute directions of the principal axes, and so there are equivalent relationships between several sets of derived polar and azimuthal angles, such as $(\theta\lambda, \phi_\lambda)$ and $(180-\theta_\lambda, 180+\phi_\lambda)$. A Fortran program HFCC-NQC has been written to make the above transformations and to calculate the nuclear quadrupole tensor **P** from EFG tensor **V**.

D. Defects as free radicals

We have also performed a few molecular calculations for free radicals $[BO_3]^{2-}$, $[BO_2]^0$, and $[BO_4]^{4-}$, using B3PW91/6-311G** implemented in Gaussian 09.[48] The results from these calculations, including nuclear hyperfine and quadrupole coupling constants based on the fully optimized geometries, are compared with results of their counterparts in the crystalline matrices.

III. RESULTS AND DISCUSSION

A. Structures for perfect crystals

The hybrid functional P-B3PW[35,38] with 20% HF exact exchange energy invariably yields the best cell constants and bond lengths for the perfect structures of calcite and zircon. For example, the cell constants and bond lengths of calcite from our P-B3PW calculations are in better agreement with data from the synchrotron XRD analysis[49] than the B3LYP results.[50] Also, the calculated cell volume for zircon is within 1% of the XRD experimental data.[51]

In addition, P-B3PW reproduces the magnitude and direction of **P** for nucleus[43]Ca in calcite determined by solid-state NMR.[52] For example, the calculated C_Q and η_Q values of −1.305 MHz and 0 agree with the NMR values of 1.39(10) MHz and <0.05°.[52] These results for[43] Ca give us confidence for the initial P-B3PW method for reproducing the electron and spin distributions around the nuclei in calcite.

B. The classic $[BO_3]^{2-}$ radical in calcite

The initial P-B3PW calculations indicate that the classic $[BO_3]^{2-}$ radical (denoted $[BO_3]^{2-}$(I) hereafter) in calcite is planar without any out-of-plane distortion, but a small in-plane distortion with one B-O bond slightly longer than the other two (Table I) is possible.

However, P-B3PW calculations (Table I) predict that the D_{3h} geometry is more stable than the asymmetric one. Figure 1(a) shows that the spin density distribution of the p orbital clearly dovetails the D_{3h} symmetry. The most salient feature of this BOHC is that the spin population of the central B atom is slightly negative at −0.095 e, almost the same as −0.085 e derived from the EPR experiment.[26] This is also evident in the spin density contour in the BO_3 plane [dashed lines in Fig. 1(a)]. The majority of the unpaired spin is equally distributed among the three O atoms with somewhat more spin on the longest B-bonded O (Table I) if the center adopts an asymmetric geometry, and the spin density on the B nucleus is −0.0178 $e/bohr^3$ ($2\times2\times2$ supercell), the same as the symmetric geometry (Table I). Therefore, this type of center, including the isoelectronic $[CO_3]^-$ and $[NO_3]^0$ radicals, can be written as O_3^{5-} to distinguish from other tri-oxygen species such as the ozonide radical O_3^-.

The negative spin density on ^{11}B is not easily understood by the use of the atomic wave function in the early work in accounting for the spin distribution of the paramagnetic nuclei.[55] Interestingly, early EPR experiments[18] commonly derived the sign of each component of the nuclear hyperfine constants of BOHCs by comparison with the free radical molecular ion $[BO_3]^{2-}$ without certainty. In fact, this negative spin density is

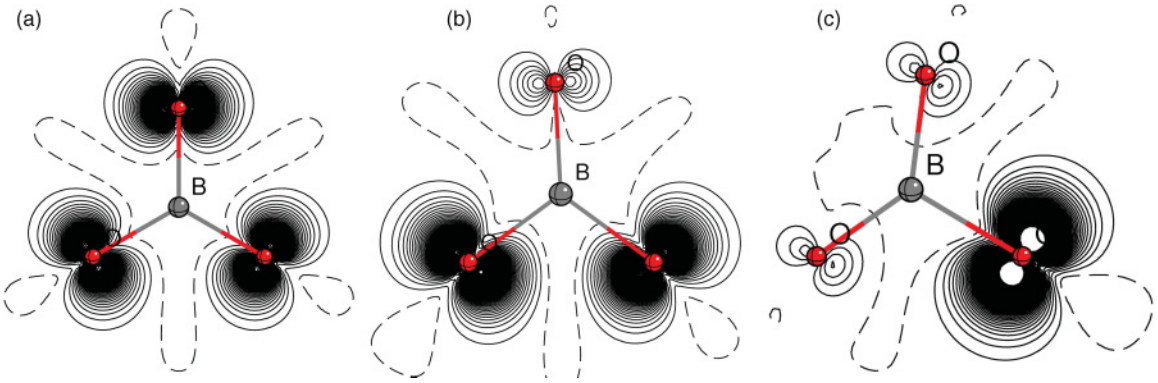

FIG. 1. (Color online) Spin densities of (a) $[BO_3]^{2-}$(I) by PBE0, (b) $[BO_3]^{2-}$(II) by PBE0, and (c) $[BO_3]^{2-}$(III) by UHF in calcite. Contours are at intervals of 0.005 $ebohr^{-3}$ and from −0.0001 and 0.315 $ebohr^{-3}$. Solid and dashed lines refer to positive and negative values, respectively.

from the effect of spin polarization that the neighboring atom (B) of the main spin atoms (O) adapts a different spin direction, i.e. negative spin (spin ↓, dashed lines in Fig. 1) on the B atom bonding to the main positive spin (spin ↑) dwelling O atoms. This effect can be effectively described by the unrestricted open-shell scheme widely implemented in modern first-principles quantum-chemical programs such as CRYSTAL.[36] In this scheme, the widely accepted concept of occupation of an electron pair in one molecular orbital or one crystal orbital is no longer rigorously valid. Spin polarization has also been found to be important in proper description of the magnetization of transition metal complexes as revealed by polarized neutron diffraction experiments.[56] The reasonable agreement between the present results and the 77 K EPR data for calcite (Table I) indicates that the unrestricted open shell P-B3PW can account for BOHCs in crystalline matrices fairly well.

Our free radical BPW91/6-311G(d,p) geometry optimization for $[BO_3]^{2-}$(I) indicates that its most stable geometry belongs to the point group D_{3h} as well. The calculated B-O bond distance is 1.3753 Å, about 0.020 Å longer than those in calcite. The ground state of this free radical is $2-A'_2$, same as that assumed four decades ago.[18] However, the spin population on B (−0.16 e) is much larger than that in calcite, indicating a notable effect of the neighboring ions on the radical in the calcite lattice.

In addition, the anisotropic *hfcc*'s from our P-B3PW calculations, particularly those from the D_{3h} symmetry, are in very good agreement with experimental results (Table I). Interestingly, however, similar to those of the expensive P-B3PW calculations, the molecular B3PW/6-311G(d,p) calculation also reproduces the EPR experimental results[26] reasonably well (Table I). This confirms that the D_{3h} $[BO_3]^{2-}$ free radical does keep its identity in calcite. Table I also shows that P-B3PW ^{11}B *nqc*'s of the $[BO_3]^{2-}$(I) center in calcite agree with available data from magic angle spin (MAS) NMR experiments.[54] The small η_Q value indicates that the $[BO_3]^{2-}$(I) center in calcite has little distortion from the ideal free radical.

C. The spin density in the D_{3h} $[BO_3]^{2-}$(I) center from density functionals

Table I shows that the a_{iso} value of the D_{3h} $[BO_3]^{2-}$(I) from our initial P-B3PW calculations with 2 × 2 × 2 supercell is 6.6% too small relative to available experimental results. Previous studies suggested that to increase the nonlocal HF exact exchange part to more than 20% is necessary to locate the $[AlO_4]^0$ hole center, and even the HF method can perform better than the well-known B3LYP series hybrid DFT method in describing the hole centers.[31] Therefore, an obvious direction to improve our results is to increase the HF exchange part in the DFT method to reduce the self-interaction problem. PBE0 was our next choice, which increases HF exact exchange to 25%, while it decreases GGA PBE exchange to 75% and keeps full PBE correlation, and it has been proven to be the most reliable DFT method for various molecular properties, including structural and hyperfine coupling constants.[37] We then increased the exact HF exchange to 50% as in Becke's half and half HHLYP/PW91. We also increased the exact HF exchange to 100% as in *ab initio* HF and in HFLYP/PW91 methods[19] as well as the HF exchange free GGA method PBE[39] as a reference to see if the hole localization of BOHCs is different from that of $[AlO_4]^0$ in α quartz.

Much more accurate integration and tighter SCF tolerances make only minimal improvements in P-B3PW *hfcc*'s. However, using LYP correlation functional improves the *hfcc*'s and thus the spin density significantly, in particular, the a_{iso} value. This may originate from the fact that the initial three parameters used in B3LYP/BPW91 have been optimized against this functional, rather than PW91.[57,58] Unfortunately, this advantage is not kept in calculations with other hybrid functionals.

HHLYP gives good results for a number of molecular properties[57] and spin distribution in the $[CoCl_4]^{2-}$ center in Cs_3CoCl_5.[56] However, its spin density for $[BO_3]^{2-}$(I) in calcite is not as good as that from B3LYP. HHLYP localizes the unpaired spin too much on the O atoms, while it overestimates the spin polarization on the B atom, resulting in too large ^{11}B hyperfine constants. Interestingly, unrestricted HF (UHF) and PBE produce the poorest spin distributions among the methods evaluated. The former localizes too much spin on the O atoms and thus about three times more spin polarization on the central B (−0.241), whereas the latter does the opposite, giving too little spin to the O atoms. Mixing only HF exact exchange with GGA correlation functional LYP as in HFLYP (i.e. UHF-LYP[19]) does not improve the situation distinctly, whose a_{iso}'s are still far too large. On the contrary, HFLYP cluster results[19] for the ^{11}B and ^{17}O hyperfine constants for

TABLE II. Calculated ^{11}B hyperfine parameters of $[BO_3]^{2-}$(I) in calcite, in mT.

Property	B3LYP	PBE0	HHLYP	HHPW	UHF	HFLYP	HFPW	PBE	Exp[a]
$A_{xx}/g_e\beta_e$	−0.798	−0.809	−0.962	−0.915	−1.553	−1.236	−1.176	−0.587	−0.83
$A_{zz}/g_e\beta_e$	−1.238	−1.255	−1.424	−1.380	−2.046	−1.730	−1.676	−0.950	−1.26
$a_{iso}/g_e\beta_e$	−0.945	−0.958	−1.116	−1.070	−1.717	−1.401	−1.343	−0.708	−0.98
$P_{xx}/g_e\beta_e$	−0.008	−0.008	−0.009	−0.009	−0.010	−0.010	−0.010	−0.007	
$P_{zz}/g_e\beta_e$	0.016	0.016	0.018	0.018	0.020	0.020	0.019	0.014	

[a]77 K EPR data from Ref. 26.

the BOHCs in B-doped SiO_2 glasses were the best overall results, and UHF also reproduced the $[AlO_4]^0$ center in silica well.[31] This is because higher HF exact exchange improves the hole localization on one O atom, whereas $[BO_3]^{2-}$(I) has a hole shared among three O atoms, and therefore a good hole localization method is not helpful. As we can see in the following, when the hole is localized on two O atoms $\{[BO_3]^{2-}$(II)$\}$ or one $\{[BO_3]^{2-}$(III) in calcite and $[BO_4]^0$ in zircon$\}$, HF and HFLYP will be much better.

In this spin equally distributed center $[BO_3]^{2-}$(I) in calcite, its 77 K EPR data is best and quantitatively reproduced by the nonempirical parameter free PBE0; the theoretical errors in the hyperfine constants are negligible (Table II).

Table III gives PBE0 ^{17}O *hfcc* values of the $[BO_3]^{2-}$(I) center in calcite, which provide direct evidence for the distribution of the unpaired spin.[59] The ^{17}O hyperfine data of the isoelectronic $[NO_3]^0$ in $NaNO_3$ (Table III) agree well with the calculated ^{17}O *hfcc*'s of $[BO_3]^{2-}$(I), indicating their similarity in spin distribution. Since the latter center has larger *hfcc*'s, we may expect the unpaired spin on the oxygen atoms of the latter to be larger, and thus the central B atom has a larger negative spin density than that in the former. This explains why the ^{14}N hyperfine structures of the $[NO_3]^0$ center was not resolved.[60] Nevertheless, Table III also shows that the spin density in the O atom in $[BO_3]^{2-}$(I) is much lower than that in the $[AlO_4]^0$ center of α quartz[59] as well as that in the $[O_2^{3-}$-$Y^{3+}]^0$ center in CaF_2 and SrF_2,[61] because its major ^{17}O *hfcc* (A_1) is much smaller than those in the latter two centers.

D. The $[BO_3]^{2-}$(II) radical in calcite

We initially intended to find the proposed $[BO_2]^0$ center in calcite,[28] but P-B3PW was not successful. Instead, our initial P-B3PW calculations obtained a diamagnetic $[BO_2]^-$ defect that is accompanied by a nearby paramagnetic $[CO_3]^-$ defect. However, the calculated $[CO_3]^-$ center has a larger spin population on the central C atom (−0.083 *e*) than that from EPR (−0.047 *e*).[62] Also, the calculated hyperfine A(^{13}C) is orthorhombic rather than axial, so this center is not the $[CO_3]^-$ radical detected by EPR. In any case, our P-B3PW calculations do not support the $[BO_2]^0$ center in calcite proposed.[28]

On the other hand, our P-B3PW calculations suggest a new $[BO_3]^{2-}$ radical in calcite. In fact, our initial P-B3PW calculations for the $[BO_3]^{2-}$(I) indicated a slight asymmetry with a difference in B-O bond distances by 0.004 Å. To explore this possibility, we used PBE0. Table IV shows that a slightly more stable (0.029 eV) asymmetrical $[BO_3]^{2-}$ in calcite has one short B-O bond of 1.326 Å and two long B-O bonds of 1.372 Å. The bond angle between the two long B-O bonds is 107.1°, and the distance between the two O atoms is only 2.21 Å, 0.2 Å shorter than the other two O-O bonds. Figure 1(b) shows that the unpaired spin is almost equally distributed between the two long-bonded O atoms. Mullikan spin population (Table IV) indicates that 99.8% spin stays on these two atoms, whereas the small spin on the other O atom roughly cancels the negative spin density on the central B atom. Therefore, this center is of the O_2^{3-} type, and its calculated

TABLE III. Comparison of calculated ^{17}O hyperfine (mT) and quadrupole parameters (C_Q in MHz) of $[BO_3]^{2-}$ and $[BO_4]^0$ centers.

	$[BO_3]^{2-}$ in Calcite			Zircon[d]	Datolite[e]	Exp[f]	Exp[g]	Exp[h]
	(I)[a]	(II)[b]	(III)[c]	$[BO_4]^0$	$[BO_4]^0$	$[NO_4]^0$	$[O_2^{3-} - Y^{3+}]$	$[AlO_4]^0$
$A_1/g_e\beta_e$	−4.816	−6.915	−12.301	−11.744	−11.235	(−)3.92	$(-)7.27_{11}$	−11.098
$A_2/g_e\beta_e$	0.517	0.398	0.330	0.598	0.729	(+)0.30	$(+)0.6_{2.5}$	1.788
$A_3/g_e\beta_e$	0.466	0.329	0.237	0.579	0.718	(+)0.30	$(+)0.6_{2.5}$	1.527
$a_{iso}/g_e\beta_e$	−1.278	−2.063	−3.911	−3.523	−3.262	(−)1.11	(−)1.69	−2.595
C_Q/h	3.391	−5.859	−12.974	−12.085	−12.007			
η_Q	0.887	0.662	0.405	0.424	0.634			

[a]PBE0 results for one O atom in the center.
[b]The average value for the almost equal PBE0 *hfcc*'s of the two spin O atoms.
[c]HHLYP results for the single spin O atom.
[d]PBE0 results for the single spin O atom.
[e]P-B3PW results for the single spin O atom.
[f]EPR data for $[NO_3]^0$ in $NaNO_3$ crystal from Ref. 60; signs are added.
[g]EPR data of $[O_2^{3-}$-$Y^{3+}]^0$ from Ref. 61, signs are added, and the subscripts are error.
[h]EPR data of $[AlO_4]^0$ from Ref. 59.

TABLE IV. Bond length (Å), spin (e), ^{11}B hyperfine parameters (mT) and formation energies (eV) of $[BO_3]^{2-}$(I), $[BO_3]^{2-}$(II), and $[BO_3]^{2-}$(III) in calcite.

	$[BO_3]^{2-}$(I)	$[BO_3]^{2-}$(II)			$[BO_3]^{2-}$(III)			
Center	PBEO	PBEO	Exp[a]	Exp[b]	HHLYP	UHF	Exp[c]	Exp[d]
r(B-O_1)	1.353	1.326			1.322	1.316		
r(B-O_2)	1.353	1.372			1.322	1.316		
r(B-O_3)	1.353	1.372			1.439	1.479		
Spin ^{1}1B	−0.103	−0.081			−0.067	−0.066		
Spin O_1	0.368	0.074			0.077	0.025		
Spin O_2	0.368	0.503			0.076	0.025		
Spin O_3	0.368	0.502			0.917	1.024		
$A_1/g_e\beta_e$	−0.809	−0.9522	(−)0.92	(−)0.978	−1.058	−1.282	-1.22_3	−1.142
$A_2/g_e\beta_e$	−0.809	−0.8585	(−)0.82	(−)0.878	−1.247	−1.389	-1.44_3	−1.427
$A_3/g_e\beta_e$	−1.255	−1.3549	(−)1.23	(−)1.315	−0.681	−0.876	-0.68_5	−0.729
$a_{iso}/g_e\beta_e$	−0.958	−1.0552	(−)0.99	(−)1.057	−0.995	−1.182	−1.11	−1.099
E_{form}^{PBE0}	1.0976	1.0684			1.2957[e]	2.3094[e]		

[a]77 K EPR data from Ref. 29; signs are added.
[b]293 K EPR data from Ref. 28.
[c]EPR data for BOHC radical I in $Li_2O.4B_2O_3$ from Ref. 3, and subscripts are experimental error.
[d]ESEEM data for crystalline B_2O_3 from Ref. 67.
[e]HHLYP and UHF geometries were used to calculate E_{form} by PBE0, refer to Eq. (9) in the text.

^{17}O hyperfine constants are indeed closely comparable to those of the $[O_2^{3-}$-$Y^{3+}]^0$ center in fluorite CaF_2.[40,61] We opt to write this center as $[BO_3]^{2-}$(II) to distinguish it from $[BO_3]^{2-}$(I), with emphasis on the B atom's true coordination of three.

The calculated spin distribution of the $[BO_3]^{2-}$(II) center well reproduces that of the $[BO_2]^0$ center from the 293 K EPR experiment.[28] In particular, the maximum PBE0 hyperfine error is only 3.04% (Table IV, 0.042 mT). This suggests that the proposed nonlinear $[BO_2]^0$ center in calcite is in fact the distorted $[BO_3]^{2-}$(II). Also, our PBE0 value of 107° supports the suggested ∠OBO angle of 105°, not the large value of 134°.[28]

E. A new $[BO_3]^{2-}$(III) center in calcite

We further wonder whether there is a $[BO_3]^{2-}$ center in calcite with the major spin localized only on one O atom. Calculations do support this center, hereafter denoted $[BO_3]^{2-}$(III) to illustrate the associated B atom and its immediate coordination environment.

Conceivably, this center can only be localized by higher HF exact exchange DFT methods (Table IV) as in the BOHCs or $[AlO_4]^0$ in α quartz.[19] This spin localized center is also planar, but distorted from D_{3h} to C_s, consisting of two short B-O bonds (1.322 Å) and one long bond (1.439 Å). The large angle between two short B-O bonds is 131.9°, due to the repulsion of the nuclei and electron densities of the two close O atoms. The long B-O bond, similar to the B-OH bond in $[BO_2OH]$ groups,[63] distinguishes this center from that proposed by Pacchioni *et al.*[19] Over 90% spin is on the long-bonded O atom and a small negative spin on the central B due to spin polarization [Fig. 1(c)]. This center is therefore a classic O^- center.[64] Indeed, the calculated ^{17}O *hfcc*'s of $[BO_3]^{2-}$(III) (Table III) are similar to those of the well-established O^- centers.[59,65,66]

There is, however, no EPR experimental data for $[BO_3]^{2-}$(III) in calcite. It is noteworthy that the EPR *hfcc*'s of a BOHC in site I in $Li_2O.4B_2O_3$ (Ref. 3) and those in crystalline B_2O_3[67] are similar to the calculated values (Table IV). Although the agreement between theory and experiment needs to be improved, theory does predict the similarity of these BOHCs in these matrices. Low exact HF exchange DFT methods (B3LYP and PBE0) fail to localize this structure just as this spin strongly localized $[AlO_4]^0$ in α quartz[65] can only be found by high exact HF exchange DFT methods, such as HHLYP/PW91.[68] Interestingly, Symons interpreted the EPR spectra of the BOHC in site I in $Li_2O.4B_2O_3$ to be a structure similar to the D_{3h} BOHC, whereas Griscom *et al.* suggested a four-coordinated ≡B-O• center with the unpaired spin localized on a single O atom.[69,70]

To compare the stability of the three BOHCs,[71] we calculated their formation energies (E_{form}) using PBE0 because it gives the best spin density distribution as shown above:

$$E_{form} = E_{BOHC} - (E_{calcite} + \mu_B - \mu_C), \quad (9)$$

where E_{BOHC} and $E_{calcite}$ denote the total energies of a BOHC, such as $[BO_3]^{2-}$(II) and the perfect calcite crystal, both in the $2 \times 2 \times 2$ supercell (Tables IV). The last two terms are the chemical potentials of atoms B and C, respectively, approximated by the open-shell PBE0 total energies of the atomic ground states.

The most stable BOHC in calcite is $[BO_3]^{2-}$(II), which is more favorable than the classic D_{3h} $[BO_3]^{2-}$(I) and the novel $[BO_3]^{2-}$(III) by 0.029 and 0.227 eV, respectively (Table IV). Table IV also shows that the two short bonds of the $[BO_3]^{2-}$(III) structure given by UHF are too short (1.319 Å), whereas the third bond of 1.479 Å is too long in comparison with the known range of three-coordinate B-O bond distances from 1.322 to 1.428 Å.[72] Since the formation energy of this BOHC is the highest among the three BOHCs in calcite, we

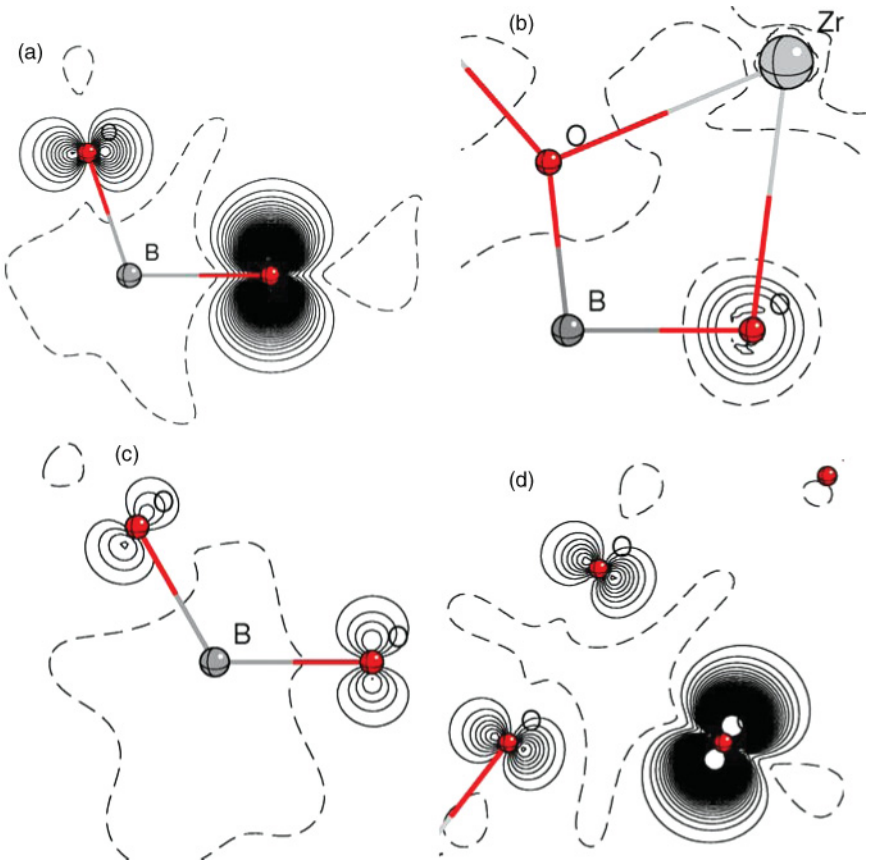

FIG. 2. (Color online) The P-B3PW spin densities of $[BO_4]^0$ in zircon in five planes: (a) O_1BO_4, (b) O_3BO_4, (c) O_1BO_3, and (d) $O_1O_2O_4$ planes. O_4 has the most spin, ~80%, and O_1 and O_2 each has ~8% spin, while O_3 has the least spin, ~5%. The C_s symmetry plane passes through the O_3BO_4 plane.

can expect that its formation would take more effort, such as a proper precursor and/or strong irradiation. On the other hand, the small energy difference with the most stable $[BO_3]^{2-}$(II) suggests that its formation is still probable under ambient experimental condition. However, there is no experimental evidence for the presence of more than one $[BO_3]^{2-}$ center in any natural or synthetic calcite.

F. The $[BO_4]^0$ center in zircon

The Si atom in the ideal zircon structure has a site symmetry D_{2d}, whereas the $[BO_4]^0$ center, as determined by 15 K EPR experiments, has been shown to exhibit an m (C_s) symmetry.[25] P-B3PW calculations of the $[BO_4]^0$ center in zircon confirm its C_s symmetry and show it to arise from nonequivalent B-O bonds (Table V, Fig. 2). In particular, one B-O bond is 0.133 Å longer than the other three bonds. This B-O bond of ~1.60 Å (Table V) considerably exceeds the usual range of 1.45–1.50 Å (mean 1.48 Å) from typical BO_4 groups in borates.[72]

The majority (~80%) of the unpaired spin is localized on the long-bond O atom, whereas the remaining unpaired spin is distributed among the other three O atoms. This also reflects the C_s symmetry of this defect structure as revealed by the EPR experiment[25] and can be seen more clearly in the spin density contour [Figs. 2(a), 2(b), and 2(d)]. Also, the $[BO_4]^0$ center in zircon is characterized by a small negative spin (−0.044 e) on the central B atom, closely comparable to that (−0.0504 e) estimated from the EPR experiment. This spin polarization is demonstrated by the dashed-line surrounding areas, where the central B atom locates, in Fig. 2. As expected, the main spin locates in the O_4 $2p_z$ orbital that is normal to the plane O_3BO_4 [Figs. 2(a) and 2(b)]. It should be noted that from Walsby

TABLE V. Bond length (Å), spin (e), and ^{11}B hyperfine (mT) and quadrupole (C_Q in MHz) parameters of $[BO_4]^0$ in zircon.

	Zircon		Datolite	
Property	EPR[a]	2×2×2[b]	EPR[c]	1×2×2[c]
r(B-O_1)		1.463		1.466
r(B-O_2)		1.463		1.496
r(B-O_3)		1.471		1.457
r(B-O_4)		1.598		1.481
Spin B	(−)0.050	−0.044		−0.034
Spin O_1		0.088		0.021
Spin O_2		0.088		0.065
Spin O_3		0.050		0.005
Spin O_4		0.796		0.862
$a_{iso}/g_e\beta_e$	−0.3994	−0.5509	−0.772	−0.7613
$T_1/g_e\beta_e$	0.2090	0.1833	0.347	0.3328
$T_2/g_e\beta_e$	−0.0890	−0.0812	−0.151	−0.1400
$T_3/g_e\beta_e$	−0.1199	−0.1021	−0.196	−0.1928
C_Q/h	1.3788	1.1531		0.3603
η_Q	0.1463	0.1118		0.4665

[a]15 K EPR data from Ref. 25, and sign in parenthesis is added.
[b]Supercell P-B3PW with default grid and initial tolerances from this work.
[c]10 K EPR data and P-B3PW results from Ref. 21.

et al.'s EPR experiment,[25] only 5.04% positive unpaired spin on the central B atom can be derived because they used the simple Morton and Preston model[55] that does not account for spin polarization.

Table V also shows that the geometry of the $[BO_4]^0$ center in zircon is considerably different from its counterpart in datolite, where the four B-O bonds differ by less than 0.035 Å and are close to those of ideal BO_4 tetrahedral groups.

The P-B3PW anisotropic *hfcc* values are in excellent agreement with those determined from EPR experiments, and the calculated a_{iso} values are in broad agreements as well (Table V). Similarly, the P-B3PW *nqc* quantitatively reproduce the 15 K EPR data.[25] The EPR C_Q/h value of the $[BO_4]^0$ center in zircon, reproduced well by the P-B3PW calculation, is larger than 1 MHz, providing additional support for the significant distortion of this defect toward the BO_3 coordination.[71]

The theoretical P-B3PW directions for both *hfcc* (A_1, A_2, and A_3) and *nqc* tensors for the $[BO_4]^0$ center in zircon are also congruent with the EPR data (Table VI). Errors in the former were slightly larger than the latter, and the largest error was only 3.3° for θ of A_1 and A_3. Moreover, the calculated polar and azimuthal angles for B-O_4 are 126.9° and 180.0°, which are close to those of the unique A and P axes (Table VI). This indicates that P-B3PW reproduces the EPR observation that the unique A and P axes both extend along the B-O_4 bond direction.[25] Therefore, our DFT calculations unequivocally provide confirmation for the geometry, orientation, and electronic structure of the unusual $[BO_4]^0$ center in zircon, as suggested in the 15 K EPR experiment.[25]

G. Is PBE0 still the best DFT method for $[BO_4]^0$ in zircon?

Similar to the $[BO_3]^{2-}$(III) center in calcite, the $[BO_4]^0$ center in zircon is in effect an O^- type with the majority of the unpaired spin localized on a single O atom. Not surprisingly, the calculated ^{17}O *hfcc*'s of the $[BO_4]^0$ center are similar to those of the $[BO_3]^{2-}$(III) center in calcite and other well-established O^- centers (i.e. α quartz $[AlO_4]^0$, Table III).[59]

Though P-B3PW reproduces the 15 K EPR anisotropic hyperfine data for zircon $[BO_4]^0$ quite well, it overestimates ^{11}B a_{iso} by 38% (Table V). We then sought to reduce the discrepancy by using other DFT methods (Table VI). Change correlation from PW91 to LYP (B3LYP, Table VI) makes the calculated a_{iso} value even worse, contrary to that for calcite $[BO_3]^{2-}$(I) and $[BO_3]^{2-}$(II) centers (Tables II and IV). This may be explained by the larger electrostatic interaction between $[BO_4]^0$ and the two nearest Zr^{4+} cations (B-Zr^{4+} distances, 2.80 and 3.05 Å) in zircon than that between $[BO_3]^{2-}$ and its two nearest Ca^{2+} cations (B-Ca^{2+} distances, ~3.23 Å) in calcite. In other words, calcite $[BO_3]^{2-}$ is more molecular or freer in character than the zircon $[BO_4]^0$. Consequently, the former can be better described by B3LYP whose parameters have been determined by optimizing molecular properties.[35]

Nevertheless, our extensive test of DFT and *ab initio* HF methods reveals that B3LYP and B3PW are still the second best to PBE0 (Table VI) in the description of both the geometry and the spin distribution of the $[BO_4]^0$ center in zircon. It appears that other DFT methods with higher (>25%) HF exact exchange components create an imbalance of the exchange and correlation. In other words, for BOHCs considered in this paper, the so-called self-interaction correction cannot be overcome by simply increasing the HF exact exchange. Table VI shows that such increase even deteriorates the P-B3PW reasonable description of the dipole interaction of the unpaired electron spin and the ^{11}B magnetic nucleus (anisotropic *hfcc*'s). This is because electron correlation, the most difficult and the most complicated problem in modern theoretical chemistry, is not linear with the HF exact exchange. The over-bonding problem of the *ab initio* HF and DFT

TABLE VI. ^{11}B hyperfine and quadrupole parameters (mT) and directions (°) of $[BO_4]^0$ in zircon.

Property	B3LYP	PBE0	HHLYP	UHF	HFLYP	Exp[a]
$A_1/g_e\beta_e$	−0.3592	−0.2227	−0.4077	−0.3837	−0.3678	-0.1904_3
$A_2/g_e\beta_e$	−0.6138	−0.5034	−0.8041	−0.7237	−0.7686	-0.4884_3
$A_3/g_e\beta_e$	−0.6367	−0.5282	−0.7167	−0.6709	−0.7058	-0.5193_2
$a_{iso}/g_e\beta_e$	−0.5366	−0.4181	−0.6428	−0.5928	−0.6141	−0.3994
θ_1	132.4	128.4	125.2	121.9	122.8	128.9_1
ϕ_1	180.0	180.0	180.0	180.0	180.0	180
θ_2	90.0	90.0	89.7	90.0	89.9	90
ϕ_2	90.0	90.0	90.2	90.0	90.1	90
θ_3	137.6	139.6	144.8	148.1	147.2	141.1_1
ϕ_3	0.0	0.0	0.6	0.0	0.2	0
$P_1/g_e\beta_e$	0.0077	0.0097	0.0068	0.0105	0.0092	0.0082_2
$P_2/g_e\beta_e$	−0.0035	−0.0046	−0.0035	−0.0048	−0.0041	-0.0035_2
$P_3/g_e\beta_e$	−0.0042	−0.0052	−0.0034	−0.0057	−0.0050	-0.0047_2
θ_1	122.5	122.3	115.4	117.3	117.2	120.9_7
ϕ_1	0.0	0.0	0.0	0.0	0.0	0
θ_2	90.0	90.0	90.7	89.9	89.9	90
ϕ_2	90.0	90.0	89.7	90.1	90.0	90
θ_3	147.5	147.7	154.6	152.7	152.8	149.1_7
ϕ_3	180.0	180.0	178.2	180.3	180.2	180

[a]15 K EPR data from Ref. 25, and signs are added.

methods with high HF exact exchange components gives anomalously short average B-O bonds, particularly those without DFT exchange components, such as HFLYP that did account for the $[AlO_4]^0$ in silica well.[31,69] These methods also significantly spoil the theoretical directions of the hyperfine principal axes of the $[BO_4]^0$ center in zircon, indicating their inadequacy in predicting the orientation of the defect magnetization.

PBE0 gives a much longer hole-trapping B-O bond (1.678 Å) than these methods, and the unpaired electron spin on the B atom is also lower ($-0.035\ e$). The spin on the hole O atom gets to 0.911 e. Analogous to $[BO_3]^{2-}$(I) and $[BO_3]^{2-}$(II) in calcite, PBE0 still best reproduces the 15 K EPR data for the $[BO_4]^0$ center in zircon.[25] The calculated ^{11}B a_{iso} error is only 0.019 mT (4.7%, Table VI), and the biggest angle discrepancy is 1.5°. Again, PBE0 is the best DFT method for the $[BO_4]^0$ center in zircon. Therefore, we recommend PBE0 for the calculations of boron paramagnetic defects in solids.

H. Implications for BOHCs in glasses and other materials

Numerous previous studies have established the complexity of radiation-induced BOHCs in glasses and other materials. In binary alkali borosilicate glasses, for example, there are $BOHC_1$ and $BOHC_2$ with slightly different EPR spectra (5-line and 4-line) depending on the molar percentage of the alkali oxide (⟨ or ⟩ 25 mol%) and silica.[3,6,11–14,18,19,25,70,71] $BOHC_1$ is observed only in v-B_2O_3 and low alkali oxide glasses, whereas $BOHC_2$ is observed in high alkali oxide glasses. Griscom *et al.*'s initial bridging oxygen model[3,4] for BOHCs has been disproved. Modern techniques such as ENDOR, ESEEM, and HYSCORE spectroscopy's, and DFT methods, mainly the clusters approach and only sporadically supercell ones, have been used to reveal the atomistic structure and spin distribution of these BOHCs. At present, $BOHC_1$ is believed to be strongly distorted [$^-$O$_3$B-O$^\bullet$—BO$_3^-$] in danburite,[7] and = B-O$^\bullet$ in borosilicate glasses.[13] Based on 1D-ESEEM and 2D-HYSCORE spectra of the B_2O_3 glass and theoretical calculations, Deligiannakis *et al.*[67] proposed three $BOHC_1$ models, $BOHC_{1\alpha}$, $BOHC_{1\beta}$, and $BOHC_{1\gamma}$, but in all of them the unpaired spin is localized on an O atom, that is, network-bound [-O-]$_2$B-O$^\bullet$. $BOHC_2$ is commonly believed to be an orthoborate group model, like our $[BO_3]^{2-}$(II) in calcite, $-[BO_2^{2-}]$ with major spin density shared by two nonbridging O atoms.[6,73] However, the atomistic and electronic structures are frequently complicated; accurate theoretical calculation is indispensible to solve the BOHC-related problems and to properly interpret the EPR spectra.[11,15,21]

Our recognition of three distinct types of $[BO_3]^{2-}$ centers in calcite and confirmation of the unusual $[BO_4]^0$ center in zircon are obviously useful for interpretation of powder EPR spectra of BOHCs in glasses and other materials. The $[BO_4]^0$ center is distinct from other BOHCs in its small ^{11}B hyperfine constants, which may be difficult to resolve in powder EPR spectra. The $[BO_3]^{2-}$(I) and (II) centers are more difficult to distinguish on the basis of their ^{11}B hyperfine constants, although their ^{17}O hyperfine constants are distinct but are usually not available owing to the exceedingly low natural abundance of this isotope. Similarly, the magnitudes of the ^{11}B hyperfine constants of the $[BO_3]^{2-}$(I) and (II) centers are similar to those of the common $[BO_4]^0$ center. Obviously, caution must be exercised in interpretation of powder EPR spectra of BOHCs in glasses and other materials.

Finally, the formation of the three distinct types of $[BO_3]^{2-}$ centers in calcite may be linked to different diamagnetic precursors. For example, the $[BO_3]^{2-}$(I) center is probably attributable to the common occurrence of the symmetrical $[BO_3]^{3-}$ group.[72] On the other hand, the $[BO_2(OH)]^{2-}$ group with a long B-OH bond and two short B-O bonds would be an ideal candidate for the formation of the $[BO_3]^{2-}$(III) type center.[63] Considering the three distinct types of $[BO_3]^{2-}$ centers, it is surprising that there appears to be no report of any $[BO_4]^0$ type centers with the unpaired spin distributed on more than one oxygen atom.

IV. CONCLUSIONS

The electronic structures, nuclear hyperfine coupling constants, and nuclear quadrupole parameters of fundamental boron oxygen hole centers in zircon ($ZrSiO_4$, $I4_1/amd$) and calcite ($CaCO_3$, $R\bar{3}c$) have been examined using all-electron supercell HF and DFT methods. Some of these methods are effective to account for the electronic structures of BOHCs in crystals. The following conclusions may be drawn:

(1) Three distinct ($S = 1/2$) $[BO_3]^{2-}$ centers in calcite have been found: the classic $[BO_3]^{2-}$(I) with D_{3h} symmetry and the unpaired spin equally distributed among the three O atoms (i.e. the O_3^{5-} type); $[BO_3]^{2-}$(II), the previously reported $[BO_2]^0$ center with the equally distributed unpaired spin between two long B-O bonded O atoms (O_2^{3-}); and $[BO_3]^{2-}$(III), a new variety with its ∼90% unpaired spin localized on the single long B-O bonded (1.44 Å) O atom (O^-). The formation of distinct $[BO_3]^{2-}$ centers is attributable to the geometric differences of their diamagnetic $[BO_3]^{3-}$ precursors.

(2) Results confirm the unusual highly distorted $[BO_4]^0$ center in zircon with major unpaired electron spin on the long B-O bonded (1.68 Å) oxygen atom.

(3) These BOHCs are all characterized by a small negative spin on the central B atom due to spin polarization.

(4) The nonempirical parameter free PBE0 is the best DFT method for description of the electronic structures of the BOHCs in this paper. It reproduces both the 15 K EPR magnitudes and directions of ^{11}B hyperfine coupling tensors and the nuclear quadrupole tensors for the $[BO_4]^0$ center in zircon quantitatively.[25] It also reproduces the ^{11}B hyperfine coupling constants of the $[BO_3]^{2-}$(I) and $[BO_3]^{2-}$(II) centers in calcite quantitatively.

(5) This work provides new insights into BOHCs in glasses and amorphous materials.

ACKNOWLEDGMENTS

We thank Natural Science and Engineering Research Council of Canada for financial support. DFT calculations in this research have been enabled by the use of Westgrid computing resources, which are funded in part by the Canadian Foundation for Innovation, Alberta Innovation and Science, BC Advanced Education, and the participating research institutions. Westgrid equipment is provided by IBM, Hewlett Packard, and SGI.

*Corresponding author: zuchengli@gmail.com
†yuangming.pan@usask.ca

[1]E. L. Yasaitis and B. Smaller, Phys. Rev. **92**, 1068 (1953).
[2]S. Lee and P. J. Bray, J. Chem. Phys. **39**, 2863(1963); **40**, 2982 (1964).
[3]D. L. Griscom, P. C. Taylor, D. A. Ware, and P. J. Bray, J. Chem. Phys. **48**, 5158 (1968).
[4]D. L. Griscom, G. H. Sigel Jr., and R. J. Ginther, J. Appl. Lett. **47**, 960 (1976).
[5]W. J. Weber, R. C. Ewing, C. A. Angell, G. W. Arnold, A. N. Cormack, J. M. Delaye, D. L. Griscom, L. W. Hobbs, A. Navrotsky, D. L. Price, A. M. Stoneham, and M. C. Weinberg, J. Mater. Res. **12**, 1946 (1997).
[6]I. A. Shkrob, B. M. Tadjikov, and A. D. Trifunac, J. Non-Cryst. Solids **262**, 6 (2000).
[7]I. A. Shkrob and V. F. Tarasov, J. Chem. Phys. **113**, 10723 (2000).
[8]Y.-F. Ruan, H. Nakao, and T. Sasaki, Chin. Phys. Lett. **17**, 896 (2000).
[9]N. K. Porwal, R. M. Kadam, T. K. Seshagiri, V. Natarajan, A. R. Dhobale, and A. G. Page, Radiat. Meas. **40**, 69 (2005).
[10]G. Kordas, J. Non-Cryst. Solids **260**, 75 (1999).
[11]G. Kordas, Phys. Rev. B **68**, 024202 (2003).
[12]G. Kordas, J. Non-Cryst. Solids **345&346**, 45 (2004).
[13]G. Kordas, J. Non-Cryst. Solids **351**, 2358 (2005).
[14]R. M. Kadam, T. K. Seshagiri, V. Natarajan, and S. V. Godbole, Phys. Res., Sect. B **266**, 5137 (2008).
[15]G. Kordas and D. Goldfarb, J. Chem. Phys. **129**, 154502 (2008).
[16]B. D. Parkinson, D. Holland, M. E. Smith, M. E. Howes, and C. R. Scales, J. Non-Cryst. Solids **353**, 4076 (2007).
[17]M. Mohapatra, R. M. Kadam, B. S. Tomar, R. K. Mishra, C. P. Kaushik, S. V. Godbole, K. Raj, and V. K. Manchanda, Mater. Sci. Eng. **2**, 012022 (2009).
[18]P. C. Taylor, D. L. Griscom, and P. J. Bray, J. Chem. Phys. **54**, 748 (1971).
[19]G. Pacchioni, M. Vezzoli, and M. Fanciulli, Phys. Rev. B **64**, 155201 (2001).
[20]R. Carboni, G. Pacchioni, M. Fanciulli, A. Giglia, N. Mahne, M. Pedio, S. Nannarone, and F. Boscherini, Appl. Phys. Lett. **83**, 4312 (2003).
[21]R. Li, Z. Li, M. Mao, and Y. Pan, Phys. Chem. Minerals **38**, 33 (2011); U. Gerstmann, M. Amkreutz, and H. Overhof, Phys. Status Solidi **217**, 665 (2000).
[22]L. V. Bershov and V. O. Martirosyan, Soviet Phys. Crystallogr. USSR **14**, 823 (1970).
[23]S. K. Misra, J. Bandet, C. Bacquet, and T. E. McEnally, Phys. Status Solidi. A Appl. Res. **80**, 581 (1983).
[24]A. I. Novozhilov, S. P. Nosv, G. A. Gorbacheva, and M. I. Samoilovich, Mineral. Zh. **10**, 1988 (in Russian, 1988).
[25]C. J. Walsby, N. S. Lees, W. C. Tennant, and R. F. C. Claridge, J. Phys. Condensed Matter **12**, 1441 (2000).
[26]R. S. Eachus and M. C. R. Symons, J. Chem. Soc. A: Inorg., Phys., Theoret. **10**, 2438 (1968).
[27]W. C. Tennant, R. F. C. Claridge, C. J. Walsby, and N. S. Lees, Phys. Chem. Minerals **31**, 203 (2004).
[28]G. Bacquet, J. Dugas, and C. Belin, Magn. Reson. Relat. Phenom., Proc. No. Congr. AMPERE, 18th (Nottingham) **1**, 161 (1975).
[29]L. V. Bershov and A. S. Marfunin, Geokhimya **3**, 446-9 (in Russian, 1981).
[30]C. Pisani, *Quantum-Mechanical Ab-Initio Calculation of the Properties of Crystalline Materials, Lecture Notes in Chemistry*, vol. 67 (Springer Verlag, Berlin, 1996), p. 47.
[31]J. Lægsgaard and K. Stokbro, Phys. Rev. Lett. **86**, 2834 (2001); G. Pacchioni, F. Frigoli and D. Ricci, **63**, 054102 (2000).
[32]J. To, A. A. Sokol, S. A. French, K. Kaltsoyannis, and C. R. A. Catlow, J. Chem. Phys. **122**, 144704 (2005).
[33]R. Dovesi and R. Orlando, Phase Transitions: A Multination. J. **52**, 151 (1994).
[34]C. Freyria-Fava, F. Dovesi, V. R. Saunders, M. Leslie, and R. Roetti, J. Phys. Condens. Matter **5**, 4793 (1993).
[35]A. D. Becke, J. Chem. Phys. **98**, 5648 (1993).
[36]R. Dovesi, V. R. Saunders, C. Roetti, R. Orlando, C. M. Zicovich-Wilson, F. Pascale, B. Civalleri, K. Doll, N. M. Harrison, I. J. Bush, Ph. D'Arco, and M. Llunell, *CRYSTAL06 User's Manual* (University of Torino, Torino, Italy, 2006), p. 1.
[37]C. Adamo and V. Barone, J. Chem. Phys. **110**, 6158 (1999).
[38]J. P. Perdew and Y. Wang, Phys. Rev. B **45**, 13244 (1992).
[39]J. P. Perdew, K. Burke, and M. Ernzerhof, Phys. Rev. Lett. **77**, 3865 (1996).
[40]S. M. Botis, D. A. Adriaens, and Y. Pan, Phys. Chem. Minerals **36**, 1 (2009); S. M. Botis and Y. Pan, Mineral. Mag. **73**, 537 (2009).
[41]L. Valenzano, F. J. Torres, K. Doll, F. Pascale, C. M. Zicovich-Wilson, and R. Dovesi, Z. Phys. Chem. **220**, 893 (2006).
[42]R. Dovesi, CRYSTAL, [http://www.crystal.unito.it/Basis_Sets/zirconium.html] (2006).
[43]C. Pisani, R. Dovesi, and R. Orlando, Int. J. Quantum Chem. **42**, 5 (1992).
[44]C. Gatti, V. R. Saunders, and C. Roetti, J. Chem. Phys. **101**, 10686 (1994).
[45]F. Weigend and R. Ahlrichs, Phys. Chem. Chem. Phys. **7**, 3297 (2005).
[46]P. Pyykko, Mol. Phys. **106**, 1965 (2008).
[47]H. Kon, Pure Appl. Chem. **61**, 2195 (1989).
[48]M. J. Frisch *et al.*, *Gaussian 09, Rev. A. 1* (Gaussian, Inc., Wallingford, CT 2009), p. 1.
[49]E. N. Maslen, V. A. Streltsov, N. R. Streltsova, and N. Ishizawa, Acta Cryst. B **51**, 929 (1995).
[50]M. Prencipe, F. Pascale, C. M. Zicovich-Wilson, V. R. Saunders, R. Orlando, and R. Dovesi, Phys. Chem. Minerals **31**, 559 (2004).
[51]R. J. Finch, J. M. Hanchar, P. W. O. Hoskin, and P. C. Burns, Am. Mineral. **86**, 681 (2001).
[52]D. L. Bryce, E. B. Bultz, and D. Aebi, J. Am. Chem. Soc. **130**, 9282 (2008).
[53]L. V. Bershov and A. S. Marfunin, Dokl. Akad. Nauk SSSR **173**, 410 (in Russian, 1967).
[54]K. Klochko, G. D. Cody, J. A. Tossell, P. Dera, and A. J. Kaufman, Geochim. Cosmochim. Acta **73**, 1890 (2009).
[55]J. R. Morton and K. F. Preston, J. Magnet. Res. **30**, 577 (1978).
[56]Z. Li, D. Jayatilaka, B. N. Figgis, and G. S. Chandler, J. Chem. Phys. **114**, 2687 (2001).
[57]A. D. Becke, J. Chem. Phys. **98**, 1372 (1993).
[58]F. Cora, M. Alfredsson, G. Mallia, D. S. Middlemiss, W. C. Mackrodt, R. Dovesi, and R. Orlando, Struct. Bond. **113**, 171 (2004).
[59]R. H. D. Nuttall and J. A. Weil, Solid State Commun. **35**, 789 (1980).

[60]A. Reuveni and Z. Luz, J. Magnet. Reson. **23**, 271 (1976).
[61]H. Bill, Helv. Phys. Acta **42**, 771 (1969).
[62]R. A. Serway and S. A. Marshall, J. Chem. Phys. **46**, 1949 (1967).
[63]S. Menchetti and C. Sabelli, Acta Cryst. B **38**, 1282 (1982); W. Sun, Y. X. Huang, Z. Li, Y. Pan, and J. X. Mi, Canadian Mineralogist **49**, 823 (2011).
[64]O. F. Schirmer, J. Phys. Condens. Matter **18**, 667 (2006).
[65]R. H. D. Nuttall and J. A. Weil, Can. J. Phys. **59**, 1696 (1981).
[66]D. F. Howarth, M. J. Mombourquette, and J. A. Weil, Can. J. Phys. **75**, 99 (1997).
[67]Y. Deligiannakis, L. Astrakas, G. Kordas, and R. A. Smith, Phys. Rev. B **58**, 11420 (1998).
[68]G. Pacchioni, J. Chem. Phys. **128**, 182505 (2008).
[69]M. C. R. Symons, J. Chem. Phys. **53**, 468 (1970).
[70]D. L. Griscom, P. C. Taylor, and P. J. Bray, J. Chem. Phys. **53**, 469 (1970).
[71]M. R. Hansen, G. K. H. Madsen, H. J. Jakobsen, and J. Skibsted, J. Phys. Chem. A **109**, 1989 (2005).
[72]R. J. Gillespie, I. Bytheway, and E. A. Robinson, Inorg. Chem. **37**, 2811 (1998); F. C. Hawthorne, P. C. Burns and J. D. Grice, Rev. Mineral. Geochem. **33**, 41–115 (1996).
[73]D. L. Griscom, *Experimental Techniques of Glass Science* (American Ceramic Society: Westerville, OH, 1993), Ch. 6, p. 161.